Gigantic jets produced by an isolated tropical thunderstorm near Réunion Island

Serge Soula, Oscar van Der Velde, Joan Montanya, Patrice Huet, Christelle Barthe, József Bór

Gigantic jets produced by an isolated tropical thunderstorm near Réunion Island

Serge Soula,[1] Oscar van der Velde,[2] Joan Montanya,[2] Patrice Huet,[3] Christelle Barthe,[4] and József Bór[5]

Received 3 January 2011; revised 1 July 2011; accepted 13 July 2011; published 4 October 2011.

[1] Five gigantic jets (GJs) have been recorded with video and photograph cameras on 7 March 2010 above an isolated tropical storm east of Réunion Island. Three of them were produced before the storm reached its coldest cloud top temperature (approximately −81°C), and two others occurred during the cloud extension. Thanks to the close distance of observation (~50 km), the luminosity within the cloud was recorded, and the events are analyzed in unprecedented detail. The tops of the GJs are estimated between 80 and 90 km. All these GJs are accompanied by long, continuous cloud illumination, and they are preceded and followed by intermittent optical flashes from the cloud, most of time without any cloud-to-ground (CG) flash simultaneously detected, which suggests they originated mainly as intracloud discharges and without any charge transfer to Earth. The CG lightning activity is observed to cease a few tens of seconds before the jets. According to ELF data recorded at Nagycenk, Hungary, the five GJs serve to raise negative charge. Their duration ranges from 333 to 850 ms. The leading jet has the most variable duration (33–167 ms) and propagates faster at higher altitudes. The trailing jet exhibits a continuous decrease of luminosity in different parts of the jet (lower channel, transition zone and, for most events, carrot sprite-like top) and in the cloud, with possible rebrightening. The lower channels (~20–40 km altitude) produce blue luminosity which decreases with altitude and become more and more diffuse with time. The transition zone (around 40–65 km) consists of bright red, luminous beads slowly going up (~10^4 m s^{-1}), retracing the initial leading jet channels.

Citation: Soula, S., O. van der Velde, J. Montanya, P. Huet, C. Barthe, and J. Bór (2011), Gigantic jets produced by an isolated tropical thunderstorm near Réunion Island, *J. Geophys. Res.*, *116*, D19103, doi:10.1029/2010JD015581.

1. Introduction

[2] Blue jets (BJs) [*Wescott et al.*, 1995, 1998, 2001] and gigantic jets (GJs) [*Pasko et al.*, 2002; *Su et al.*, 2003] are electrical discharges shooting up from a thundercloud. The GJs reach terminal altitudes within the lower ionosphere (70–90 km). They are the most rarely observed transient luminous events (TLEs) compared to elves, halos and red sprites [*Chen et al.*, 2008]. Since their discovery [*Pasko et al.*, 2002], several GJs have been detected from ground [e.g., *Su et al.*, 2003; *van der Velde et al.*, 2007, 2010] and from spacecraft experiments [*Chen et al.*, 2008; *Kuo et al.*, 2009]. Most of the time they are observed as single event within a storm, but in one reported case, five GJs were produced in less than 15 min by a thunderstorm south of Taiwan [*Su et al.*, 2003]. A large majority of the GJs observed from space occurred over maritime storms [*Chen et al.*, 2008].

[3] The first GJ observations allowed identification of three stages in the GJ evolution: the leading jet, the fully developed jet (FDJ) and the trailing jet [*Su et al.*, 2003]. The upward propagating leading jet can be considered to have a role in the GJ process equivalent to that of the stepped leader in the cloud-to-ground (CG) lightning flash, with similar velocities (~10^5–10^6 m s^{-1}). High time resolution measurements showed much larger upward velocities for the upper part of the leading jet, typically ~10^7 m s^{-1} similar to that of downward sprite streamers [*Kuo et al.*, 2009]. The trailing jet was observed to rush upward to an altitude around 60 km in ~300 ms [*Su et al.*, 2003]. It is characterized by a bright top region which forms the "transition region" [*van der Velde et al.*, 2007] and which rises with a velocity decreasing from about 10^5 m s^{-1} to a few 10^3 m s^{-1} as it approaches its maximum altitude as shown by *Su et al.* [2003]. A rebrightening of the lower channel of the GJ can be observed after the end of the trailing jet [*Su et al.*, 2003].

[1]Laboratoire d'Aérologie, Université de Toulouse, CNRS, Toulouse, France.
[2]Electrical Engineering Department, Technological University of Catalonia, Terrassa, Spain.
[3]La Maison du Volcan, Muséum de la Fournaise, Plaine-des-Cafres, France.
[4]Laboratoire de l'Atmosphère et des Cyclones, Université de la Réunion, CNRS, Météo-France, Saint-Denis, France.
[5]Geodetic and Geophysical Research Institute, Hungarian Academy of Sciences, Sopron, Hungary.

0148-0227/11/2010JD015581

[4] In a storm with a normal charge structure, the theory proposed by *Krehbiel et al.* [2008] and *Riousset et al.* [2010] predicts positive polarity for the blue jet (i.e., carrying positive charge out of the cloud) and negative polarity for the GJ (i.e., carrying negative charge upward). On the basis of the bileader process [e.g., *Mazur and Ruhnke*, 1998], this theory explains the propagation of the GJ out of the cloud after the discharge starts as an intracloud (IC) process between the unbalanced main charge regions. The midlevel negative charge (typically 7–8 km but probably higher in the tropics) is larger than the positive charge at the cloud top which is depleted by mixing with negative charge from the screening layer at the cloud boundary. *Krehbiel et al.* [2008] considers mixing of screening layer charge at the top of the cloud as the norm in the cloud structure. The GJ discharges the negative cloud region to the ionosphere symmetrically to the negative CG flash, while the blue jet discharges the cloud top positive charge to the stratosphere (<40 km altitude). The estimated negative charge amount neutralized within the cloud for a GJ event varies considerably. *van der Velde et al.* [2007] found low values of charge moment changes (CMC) associated with a GJ (<50 C km). In contrast, *Cummer et al.* [2009] estimated CMC ~10,800 C km and charge transferred ~140 C during a GJ event. Charge values ~50 C were found by *Su et al.* [2003]. In a case of positive GJ, *van der Velde et al.* [2010] estimated a negative charge transfer of ~136 C from ionosphere to cloud. A recent study by *Chou et al.* [2010] showed three categories of GJ from the analysis of ISUAL observations based on the event chronology and the spectral properties. For the first category, the GJs are of negative polarity and exhibit the typical phases. For one of these categories, the GJs start as a BJ and exhibit a positive polarity while for the last one, the GJs can have either negative or positive polarity.

[5] We report here on five GJs recently detected by video and photo cameras above a storm close to the east coast of Réunion Island in the Indian Ocean. Thanks to the proximity of the observation (about 50 km), unprecedented details and luminosity from the cloud and from different parts of the jet discharge, including very weakly luminous ones, can be analyzed. The data and the methodology are presented in section 2. Section 3 describes the results of the analysis concerning the conditions of production in terms of storm structure and lightning activity, the characteristics of the different phases of the GJs observed by the cameras, and the ELF data associated with the jet events. Section 4 is devoted to a discussion with previous results and section 5 summarizes the main conclusions issued from the analysis.

2. Methodology

[6] The site for GJ observation, at an altitude of 1600 m, is located 55° 35′ E and 21° 12′ S in Réunion Island. The sky over the site is free of light pollution. The GJ video observations were made with a CCD Sony camera KPC-350 BH (1/3″ ExView HAD CCD) equipped with a 3.5–8 mm f/1.4 lens used at 3.5 mm. Its horizontal and vertical fields of view (FOV) are 70° and 50°, respectively. The recorded videos provide series of images (30 per second) which have been deinterlaced in frames separated by 16.7 ms in order to analyze the details of the evolution of the different GJ events. The photographs used in the study were taken with a NIKON D200 equipped with an 18 mm f/3,5 AF-S NIKKOR aspheric lens. Its exposure time was 20 s and sensitivity ISO 1600 (for very low light).

[7] The cloud top temperatures are provided by the infrared channel (10.5–12.5 μm) of the geostationary Meteosat-7 satellite located at a longitude of 58°E. One image is available every thirty minutes, and the region of the storm was scanned about 8 min after the beginning of the scan. The time indicated in the charts of Figure 2 is the time at which the storm area was scanned. The resolution of the image is 4.5×5 km^2 in the area of the storm. The parallax error (about +0.0675° to south in latitude) for cloud top location is taken into account.

[8] Lightning data used in this study consists of lightning strokes located with the technique of time of group arrival (TOGA) provided by the very low frequency (VLF) global ground-based World Wide Lightning Location Network (WWLLN) [*Lay et al.*, 2007]. The WWLLN was composed of about 40 sensors around the world at the beginning of 2010 and its detection efficiency ranged from a few percents to a few tens of percent, depending on the region of the globe considered, for strokes with a peak current greater than 30 kA [*Rodger et al.*, 2006]. The peak current values for strokes are not estimated by the system. Flashes are obtained by using the minimum distance and time interval between two successive strokes of 10 km and 0.5 s, respectively. The video imagery also provides information about lightning activity, especially in terms of optical flashes which can be associated with lightning discharges.

[9] The GJ locations are assumed to be on their lines of sight (azimuth) from the observation site and to correspond to the main lightning stroke occurrences in the same period. The stars in the images are used to determine the GJ azimuths and their elevation angles. The vertical scale in all figures including GJ imagery takes into account the wide-angle distortion (perspective effect): the tops of the GJs are seen at larger distances than their bottoms. This vertical scale is valid only at the distance of the GJ and not at the shorter distance of the cloud edge.

[10] The video images were time-stamped by the computer, which during this night was not synchronized to a time signal. In order to determine the exact event time we use the video imagery which includes a set of several tens of lightning flashes. The WWLLN data are synchronized to the Global Positioning System (GPS) clock but have an unknown number of common events with the video imagery. Events from WWLLN as well as the optical flashes from the video are considered unique flash events if they are not preceded by another event in a 1 s interval. A method is developed for identification of these common events. It consists of an analysis of the distribution of all the possible time intervals $t_A - t_B$ calculated between each event of both sets (A and B). The method is applied over a period of about 1 h (17:40 to 18:40) including 92 lightning events from WWLLN and 189 video events. The number of time intervals is therefore $N_A \times N_B = 17{,}388$. For the first step of the method, the histogram of the time interval $t_A - t_B$ is displayed over 1 s bins in Figure 1. The graph of the distribution is limited here to $t_A - t_B$ between −500 and +500 s. The distribution shows random values of the frequency except for two values of the interval corresponding to 68 and 69 s, with frequency values of 65 and 14, respectively.

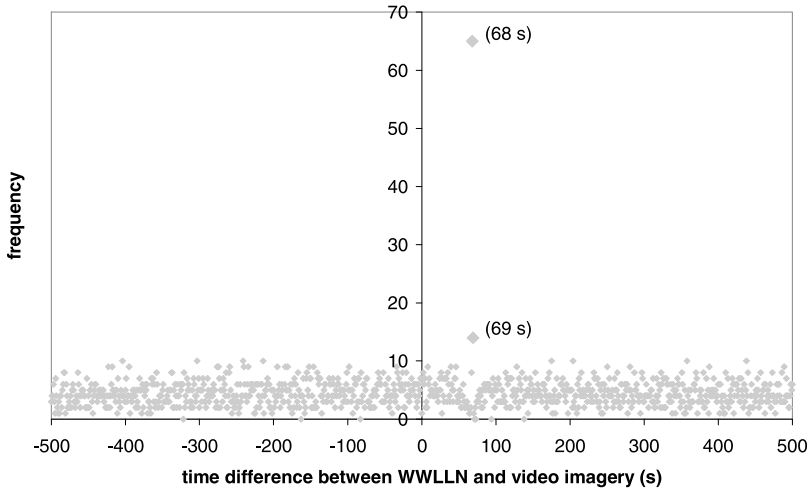

Figure 1. Frequency distribution of the time difference between the flashes detected by the WWLLN and the optical flashes provided by the video imagery.

The highest-frequency value is found when the interval $t_A - t_B$ is calculated for physically identical optical and WWLLN events, which occurs a number of times equal to the number of common events within both series of events. The time difference between the clocks of the data system lies therefore between 68 and 69 s. The second step of the method, to calculate more precisely the time difference, consists of comparing common events from both systems which have just been identified. These events are chosen to have only one stroke detected by the WWLLN to be well recognized in the video imagery. This step of the method is applied to several events and it provides a result of about 68.4 s and 68.3 s for events at the beginning and the end of the storm, respectively. For each determination the accuracy is about 20 ms (the time interval between two video frames is 16.7 ms).

[11] The correct timing allows us to look for ELF signals associated with the GJ events. Time series of the vertical electric field and the horizontal magnetic field were recorded at the Széchenyi Isván Geophysical Observatory near Nagycenk, Hungary (NCK; 47.62°N, 16.72°E) at a 514.28 Hz sampling rate with 5–30 Hz effective passband [*Sátori et al.*, 1996; *Sátori*, 2007]. ELF signals from a powerful source can be detected globally [*Williams et al.*, 2010]. Natural sources of ELF radiation are most frequently electric discharges such as the lightning flash. ELF wave packets radiated by sources of extraordinary power appear as transient, high-amplitude signals in the time series of the monitored EM field components [*Nickolaenko et al.*, 2010]. Some properties of the source discharge can be deduced by analyzing the time series of the recorded field components. For example, the polarity of the source discharge can be found by the direction of the field jump in the vertical electric (E_z) component at the onset of the event [*Hobara et al.*, 2006]. The CMC during the source discharge can be estimated from ELF data either in the time domain [*Cummer and Inan*, 2000] or in the frequency domain. Source processes cannot be followed at a fine time resolution in the NCK records owing to the relatively narrow bandwidth of the receiving system. Therefore, this analysis is carried out in the frequency domain [*Huang et al.*, 1999]. The applied method assumes that the source current moment decays exponentially in time. This is a rather simple approximation even for +CG lightning discharges, however, the CMCs calculated with this method generally do not deviate from values gained by using other procedures [*Williams et al.*, 2010]. Nevertheless, it must be noted that the calculated CMCs for the GJs have to be considered with care until the current sources for ELF radiation in GJs are explored in greater detail.

3. Results

3.1. Conditions for Production of the GJs

[12] Five GJs were recorded by the camera at 17:40:24 UT (GJ1), 17:42:49 UT (GJ2), 17:44:5 UT (GJ3), 18:26:6 UT (GJ4), and 18:29:20 UT (GJ5) on 7 March 2010. Before these five GJs, two unrecorded jets were seen with the unaided eye by the photographer (Patrice Huet) at about 17:34 and 17:36 UT and no other TLE was observed during the whole storm period. The jets were produced by an isolated storm which developed during the evening to the east of Réunion Island, as a result of converging east-northeasterly trade winds which carried warm damp air, as is usual in the tropics. The Global Forecasting System numerical weather prediction model of the National Centers for Environmental Prediction at 18:00 UT indicates 65 kg m^{-2} of precipitable water (vertically integrated water vapor), a value which is found (by the author, O.V.) only very sparsely across the tropics globally in the same model on many different days. Values of CAPE (convectively available potential energy) and various measures of vertical wind shear were elevated, but nothing out of the ordinary.

[13] Figure 2 displays cloud top temperature images from Meteosat-7 in the area of the storm (20.5°; 22° S in latitude and 55.1°; 57° E in longitude). It shows that the storm top rapidly reaches −81°C before 18:08 UT and then expands very quickly. Such low temperatures are typical for the tropopause in this region with heights which can reach 18 km [*Sivakumar et al.*, 2006]. The area with temperature lower than −70°C covers 256 km^2 at 17:38 UT, increasing to 2000 km^2 at 18:08 UT, 4900 km^2 at 18:38 UT, and 7740 km^2

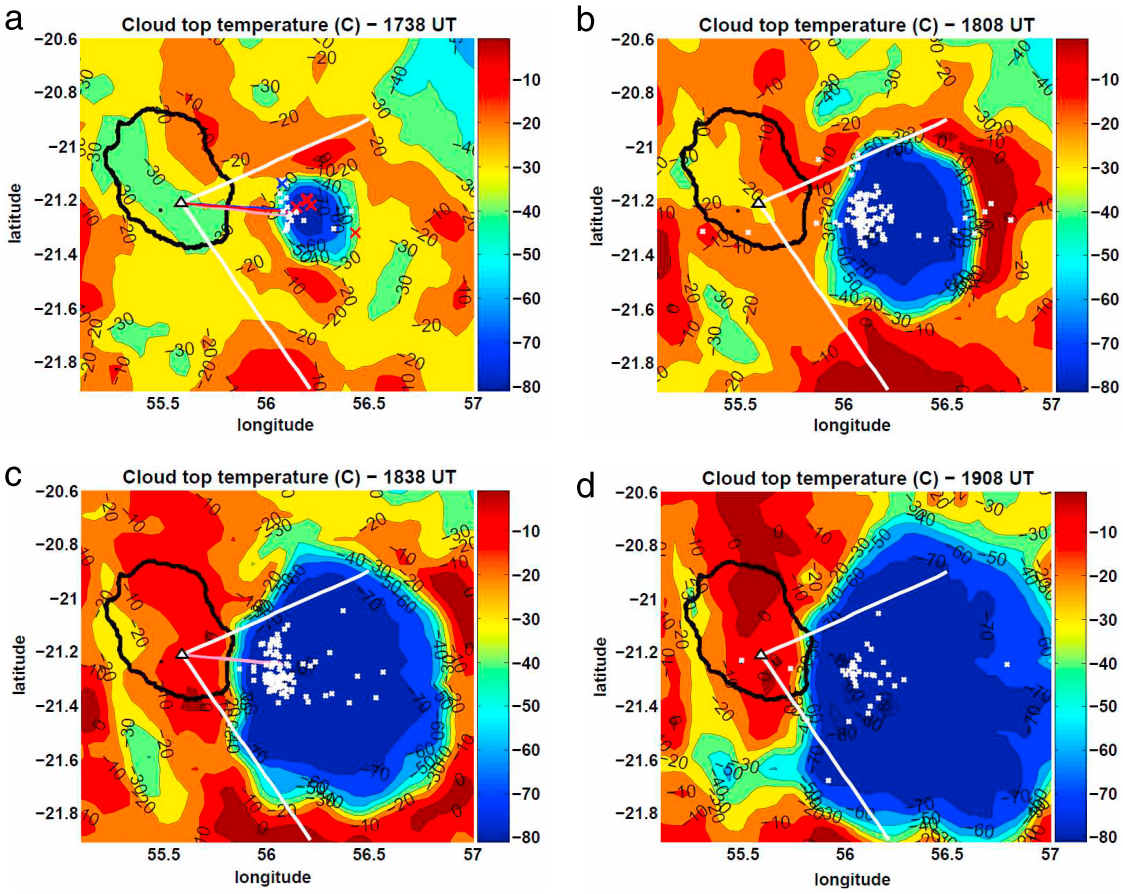

Figure 2. Charts of the cloud top temperature in the area of the GJ-producing storm at (a) 17:38 UT, (b) 18:08 UT, (c) 18:38 UT, and (d) 19:08 UT. The lightning strokes detected by the WWLLN over a 20 min period centered at the scanning time are indicated with white crosses (blue and red crosses in Figure 2a for strokes associated with GJ1 and GJ3, respectively). The triangle in Réunion Island indicates the video camera location. Lines of sight from the camera to GJ1 (blue), GJ2 (pink), and GJ3 (red) are indicated in Figure 2a, lines of sight to GJ4 and GJ5 (pink) in Figure 2c. The horizontal FOV of the camera is indicated with white lines.

at 19:08 UT. Owing to this rapid expansion, the edges of the cloud shield display strong horizontal gradients of the cloud top temperature, especially on the west side close to the east coast of Réunion Island. Figures 2c and 2d (18:38 and 19:08 UT) show several areas of minimum temperature in the cloud area which could correspond to overshooting cloud tops. Figure 2 also displays the locations of CG lightning strokes detected by the WWLLN. These locations show the western part of the cloud to be the most electrically active. The superimposed lines of sight to the GJs clearly correspond to the strongest cloud development and the main location of the strokes, especially in Figure 2c. Strokes in blue (1) and red (5) in Figure 2a were detected during the visible cloud flashes corresponding to GJ1 and GJ3, respectively. The same color is used for their lines of sight. These lines of sight do not coincide exactly with the associated strokes, especially that of GJ1 (blue color).

[14] Figure 3 displays the cumulative number of lightning parameters (strokes and flashes from WWLLN, optical flashes from the video imagery (until 18:40 UT)), the rate of the flashes detected by the WWLLN, the values of the minimum cloud top temperature, and the GJ occurrences. The detected lightning activity starts at about 17:00 UT. Before 18:00 UT the flash rate is from 1 to 2 min^{-1} with a maximum of 1.8 min^{-1} at 17:30 UT, just before the first GJs recorded by camera. At this point it should be noted that the detection efficiency of the WWLLN is much lower than any typical regional CG flash detection network [*Rodger et al.*, 2006]. In particular, the weaker flashes are missed altogether, and therefore these low rates are not representative of the true rates but can indicate a tendency. The optical flashes recorded in the video imagery start at about 17:40 UT with an arbitrary number equal to that of the WWLLN strokes. The first GJs occur within a very short period (~4 min) early in the lifetime of the storm, probably before the storm reaches its complete vertical development and before its strong horizontal expansion. From the video images and the distance to the nearest cloud edge, the cloud top altitude is estimated at 15–16 km. The average flash rate is low (~1 min^{-1}) when the three jets are produced. During an interval of 335 s (17:38:30–17:44:05 UT) preceding the third jet, only one stroke has been detected by the WWLLN. This stroke occurs about 0.5 s after GJ1. The first zoom of Figure 3 shows this period with a "plateau" for the WWLLN

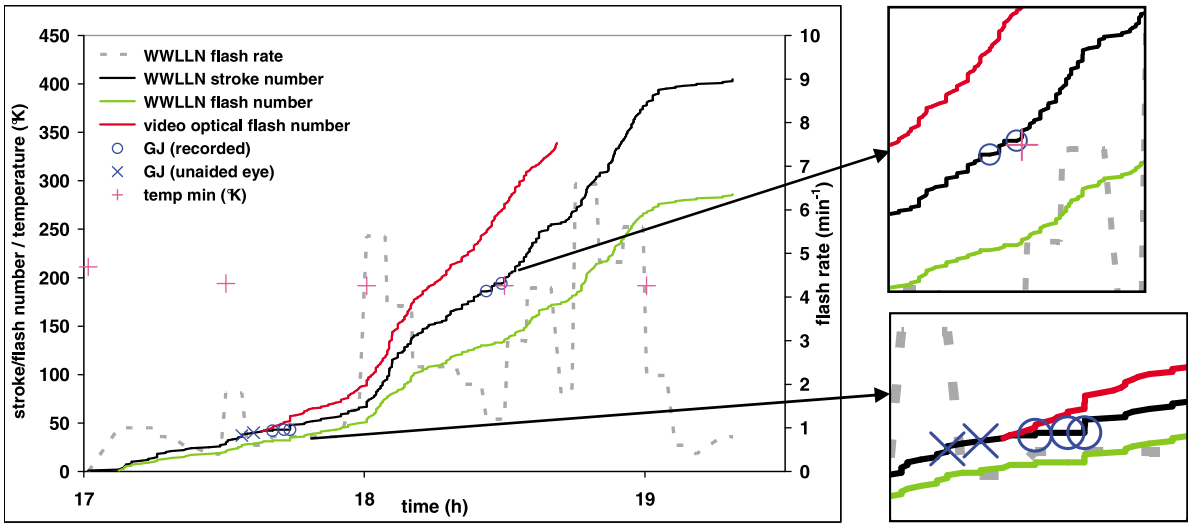

Figure 3. Time series of the flash rate (dashed line), averaged over 5 min intervals, of the cumulative number (solid lines) of strokes and flashes detected by the WWLLN and of the optical flashes detected by the video imagery. The times of the GJs observed by the camera are indicated by circles, the times of two GJs observed with the unaided eye are indicated by crosses, and the values of the temperature minimum are indicated by pluses. (right) Zooms of the periods of GJs detected by the camera.

flash number and a simultaneous and continuous increase for the optical flash number.

[15] The rates of lightning strokes and lightning flashes increase markedly after 18:00 UT. However, the flash rate fluctuates between 1.2 and 6.6 min^{-1}, probably because of new cell developments. The optical flashes show a more pronounced increase, especially after 18:30 UT, therefore probably due to IC flashes. The main stroke area (Figure 2) slightly expands and shifts to the west while stroke density increases markedly. According to the flash detection efficiency of the WWLLN in the region, which can be a few percent [*Rodger et al.*, 2006] and the stroke location in a restricted area, the flash rates (up to 6.6 min^{-1}) seems to indicate a very active storm. Two additional GJs are produced during a period of relatively low flash rate (1.2 min^{-1}). For these GJs the periods without WWLLN flashes last 136 s and 121 s. The second zoom of Figure 3 shows these periods are characterized by an increase of about 10 optical flashes estimated from the video imagery.

3.2. Characteristics of the GJs

3.2.1. Overall Description

[16] Table 1 provides an overview of the occurrence times and durations of the main phases of the GJs (leading jet, FDJ, trailing jet) and of the associated cloud luminosity. These durations which are estimated from the analysis of the video observations, are displayed in a graph in Figure 4. Table 1 also provides the estimated times of the ELF production sources and the sizes of the jets. Figure 5 displays the five GJs at different stages of development with a vertical scale estimated by taking the perspective effect into account: end of the leading jet for GJ4, FDJ for GJ2 and GJ3, beginning of the trailing jet for GJ1 and GJ5. The GJs display the characteristic shape of an inverted cone above a more collimated trunk (reaching 25–30 km altitude) at an

Table 1. Time, Duration, and Vertical Size Characteristics of the Five GJs Observed[a]

Event	GJ1	GJ2	GJ3	GJ4	GJ5
Time (UT)	17:40:24	17:42:49	17:44:05	18:26:06	18:29:20
Fully developed jet[b] (s)	24.267	50.000	05.800	06.950	20.718
ELF source[b] (s)	24.227	49.979	05.788	06.864	20.672
Futsyion og rbrny (ms)	1250	1000	1350	1370	1452
Duration of the visible GJ (ms)	850	500	333	585	550
Duration of the cloud luminosity before GJ (ms)	400	300	384	435	668
Duration of the leading jet (ms)	167	67	33	50	50
Leading jet average velocity (m s^{-1})	(0.4×10^6)	(1.0×10^6)	(2.0×10^6)	(1.2×10^6)	(1.2×10^6)
Duration of the trailing jet with beads (ms)	350	250	200	435	467
Duration of the trailing jet (no beads) (ms)	333	183	100	100	33
Duration of the cloud luminosity after GJ (ms)	–	200	633	350	234
Estimated distance (km)	53	53	53	45	45
Estimated altitude (km)	90	90	80	>80	>80

[a]The times are estimated with an uncertainty of about 20 ms. The distance and altitude are estimated with an uncertainty of about ±5 km for GJ1, GJ2, and GJ3 and ±10 km for GJ4 and GJ5.
[b]Seconds after the time of the event in hours and minutes.

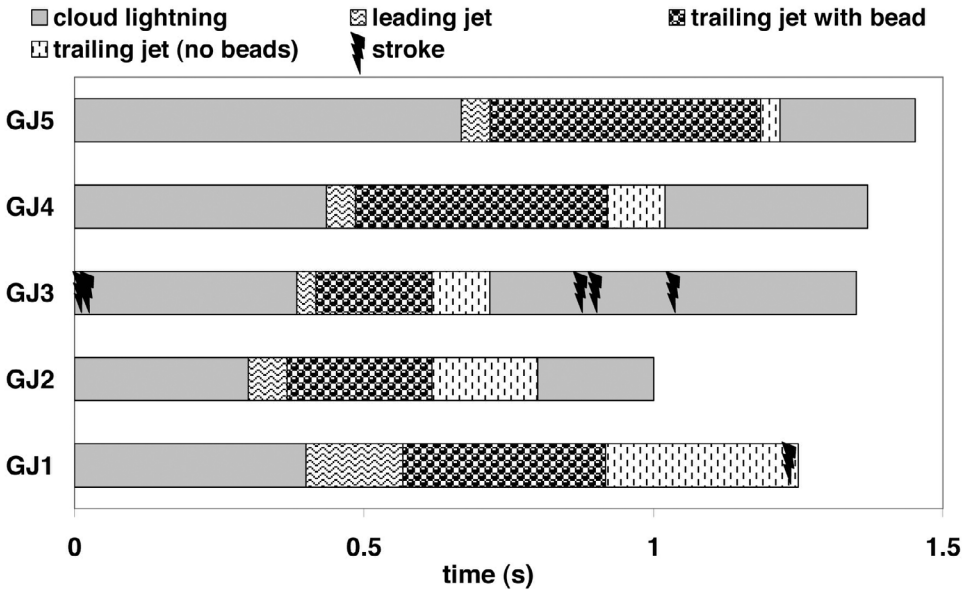

Figure 4. Comparison of the durations of the various luminous phases of each GJ event. The lightning symbols indicate occurrences of strokes detected by the WWLLN.

angle of 16° to 33° (average 23°) the largest angle being for the fourth jet. The distance from the observer is estimated at about 53 km for GJ1, GJ2 and GJ3, and 45 km for GJ4 and GJ5. The altitude estimates have large uncertainties but result in 80–90 km tops (Table 1), similar to previously reported events.

[17] The duration of the entire cloud discharges recorded in the video imagery ranges from 1 s to 1.40 s whereas the duration of the jets ranges from 0.33 s to 0.85 s. In all five events, the GJ is preceded by permanent cloud luminosity with intermittent pulses of light. Figure 6 displays for different parts of the GJ5 event and for the cloud, an evolution of the luminosity. In order to optimize the readability of the graph, the parameter considered is the ^{10}log of the number of pixels for which the luminosity exceeds a given threshold. Two values of this threshold are considered. The different graphs are provided by considering in the video imagery the upper section of the jet, its transition region, its lower section, and the visible part of the cloud. The graph of cloud luminosity clearly shows a quasi-continuous activity during the whole event, the duration of which is 1.4 s (Table 1). However, the cloud luminosity fluctuates markedly before and after the jet while it varies much more uniformly during the phases of the jet (leading jet and trailing jet). In this case (GJ5) about seven increases of luminosity can be distinguished over a period of 668 ms before the visible jet. For all jets, the duration of this initial in-cloud activity is of the order of half a second (300 to 668 ms). The cloud remains luminous during and after the visible part of the GJs, indicating continuous charge transfer.

3.2.2. Leading Jet

[18] For the five GJs, the leading jet is the most variable phase in term of duration, as seen in Table 1 and Figure 4. The leading jets always start with several channels emerging from the cloud top, some of them reaching the jet top altitude after varying lengths of time. They end with a well branched structure and a relatively low brightness, as shown for example in Figure 5 for GJ4. The duration of the leading

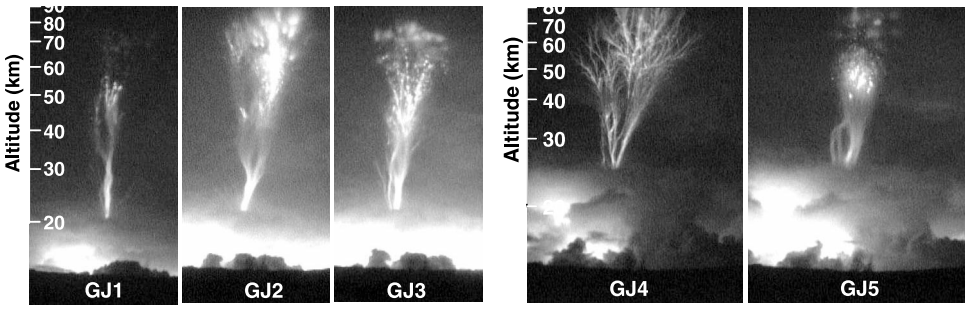

Figure 5. Images of the five GJs at different stages of their development: end of the leading jet for GJ4, FDJ for GJ2 and GJ3, and beginning of the trailing jet for GJ1 and GJ5. The vertical scale is calculated at the distance of the GJ by taking into account the perspective effect and is not valid at the distance of the cloud edge.

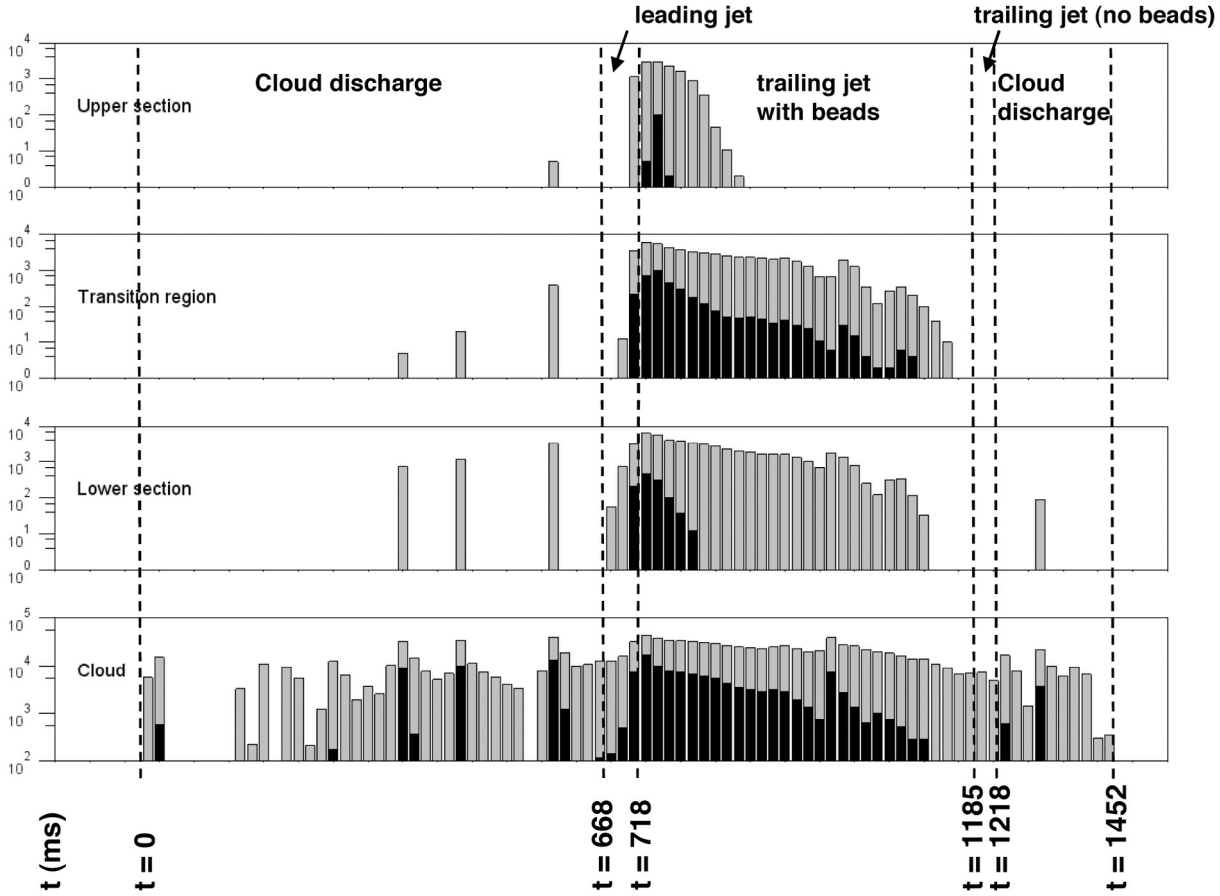

Figure 6. Time series of the number of image pixels exceeding the luminosity thresholds of 10 (gray) and 200 (black) of an 8 bit intensity scale of 0–255. The time reference $t = 0$ corresponds to the first cloud brightening of the event.

jets varies significantly from 33 ms to 167 ms (i.e., average velocity from 0.4×10^6 m s^{-1} to 2.0×10^6 m s^{-1}). Figure 7a displays 8 frames of the 10 available for the whole leading jet of GJ1 event. The whole visible vertical development is estimated at 70 km which means an average velocity of about 0.4×10^6 m s^{-1}. The multiple channels above the cloud initially rise slowly (about 0.1×10^6 m s^{-1}) and some channels accelerate and reach the maximum altitude of the jet. So, the velocity at the beginning of the leading jet is similar to that of the stepped leader in a CG flash [*Rakov and Uman*, 2003] and it can reach much larger values (>2×10^6 m s^{-1} according to Figure 7a) in its upper part. Figure 8 illustrates the development of the leading jet for GJ3 event. In this case, it is much faster as also shown in Table 1 (33 ms). The three first frames of Figure 9 show the development of the most highly branched leading jet (GJ4). Several upward channels stay below ~45 km while a larger and more branched structure (streamer-like) developed very quickly upward and out of the upper part of the camera FOV (~80 km).

[19] Figure 6 which displays the evolution of the luminosity for GJ5 event, shows that when the GJ is fully developed, its brightness and that of the cloud increases simultaneously and markedly (analogous to a "return stroke" in CG flashes). Carrot sprite-like patches of light and/or a multitude of beads can occur near the top of most events at that stage as illustrated in Figure 5 for GJ2 and GJ3. This structure of the FDJ is not always well visible, as for example in GJ1 (Figure 7b) and in GJ4 (Figure 9). In contrast, it remains for several frames in GJ3 (Figure 8) and in GJ5 (Figure 10a). The luminosity of the top of the jet seems to be related to the overall jet luminosity. Some leader channels, initially developed during the leading jet and halted in their propagation, become rapidly attached to the trunk of the jet, as shown in Figure 10a for GJ5.

3.2.3. Trailing Jet

[20] After the GJ reaches its full development and its maximum luminosity, the brightness simultaneously decreases in the most luminous parts of the jet (the main channel below 30 km, the transition region around 50 km, the diffuse patches similar to those forming the top of carrot sprites) and in the cloud. Figures 8 and 10 give a good illustration of this behavior for GJ3 and GJ5, respectively. The trailing jet consists of the lower part of the jet which remains luminous after the top parts decay. It is topped by a brighter feature, the transition region which moves up and which generally disappears before the lower channel. This phase of the jet lasts the longest and is separated into two different parts according to whether the transition region is visible or has disappeared. Table 1 gives their duration for all GJs observed. For all jets, the first part of the trailing jet (with a visible transition region) is longer than the second part, ranging from 200 ms for GJ3 to 470 ms for GJ5. The transition region consists of luminous

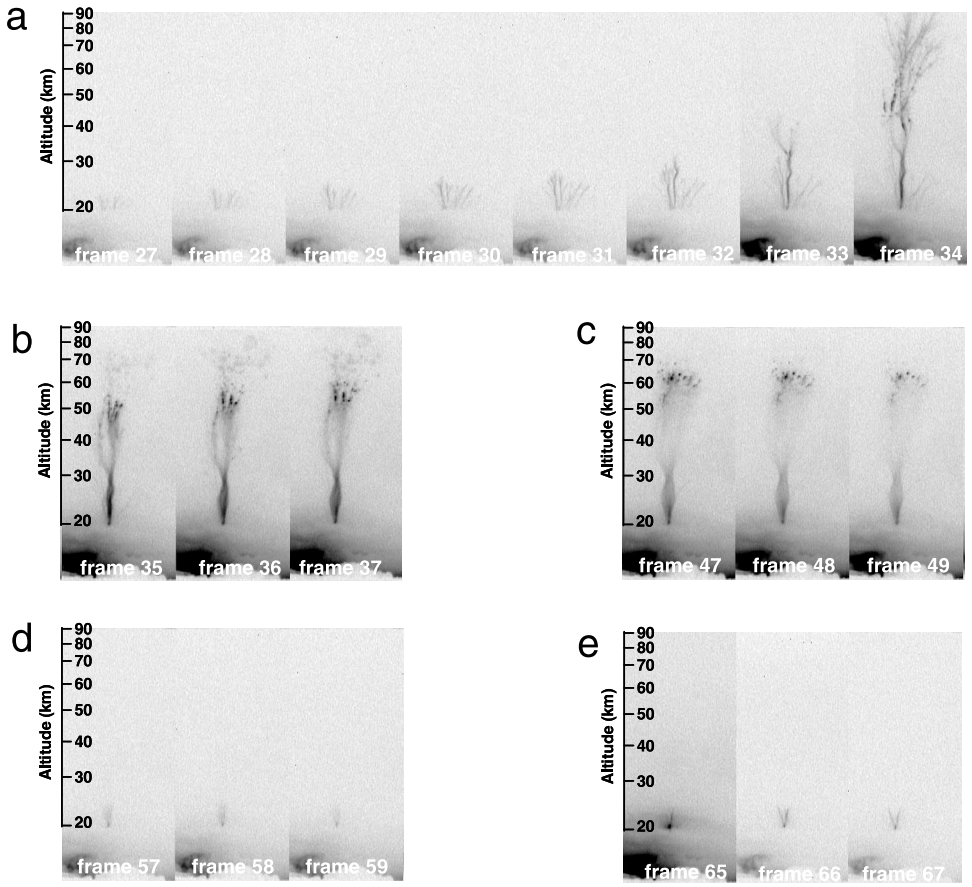

Figure 7. Series of successive de-interlaced frames from the video imagery of GJ1 in inverted color: (a) t = 434.2–567.8 ms (two frames after the beginning of the leading jet); (b) t = 567.8–617.9 ms (beginning of the trailing jet with beads); (c) t = 768.2–818.3 ms (trailing jet with beads); (d) t = 935.2–985.3 ms (trailing jet no beads); and (e) t = 1068.8–1118.9 ms (rebrightening of the lower trunk). The time reference t = 0 (frame 1) corresponds to the first cloud brightening of the event. The vertical scale is calculated at the distance of the GJ by taking into account the perspective effect and is not valid at the distance of the cloud edge.

beads slowly rising (~10^4 m s^{-1}) along leading jet channels, superimposed on a glow of varying intensity in the different GJs. Figures 7, 8, 9, and 10b illustrate this feature for GJ1, GJ3, GJ4, and GJ5, respectively. During the trailing jets of GJ4 (not shown) and GJ5 an increased brightness in the cloud (frame 60 in Figure 10b) precedes an increase of brightness of the beads and bursts of new streamers just below the beads in the transition region (frame 61 in Figure 10b). So, cloud

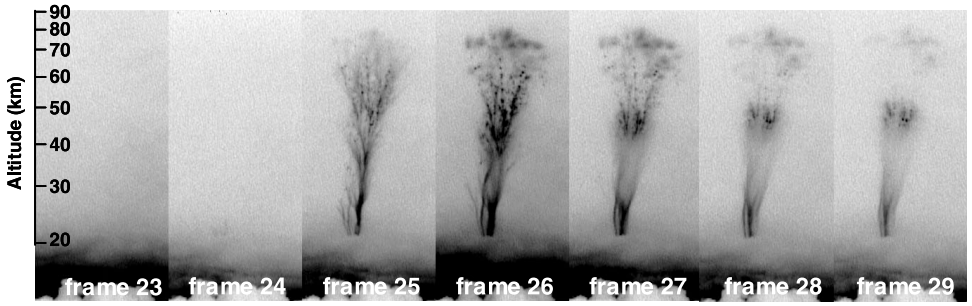

Figure 8. Seven successive de-interlaced frames from the video imagery of GJ3 in inverted color at t = 367.4–484.3 ms after the first luminosity in the cloud. The frames include cloud luminosity before jet (frame 23), leading jet (frames 24 and 25), and beginning of trailing jet (frames 26–29). The time reference t = 0 (frame 1) corresponds to the first cloud brightening of the event. The vertical scale is calculated at the distance of the GJ by taking into account the perspective effect and is not valid at the distance of the cloud edge.

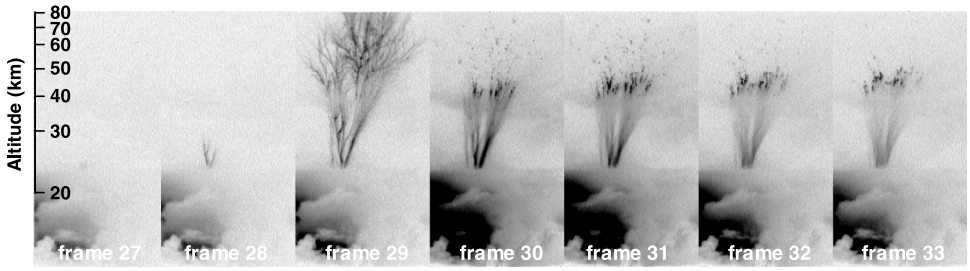

Figure 9. Seven successive de-interlaced frames in inverted color from the video imagery of GJ4, t = 434.2–551.1 ms, leading jet/beginning of the trailing jet with beads. The time reference t = 0 (frame 1) corresponds to the first cloud brightening of the event. The vertical scale is calculated at the distance of the GJ by taking into account the perspective effect and is not valid at the distance of the cloud edge.

luminosity fluctuations appear to be physically linked with the transition region brightness during the trailing jet stage.

[21] During the trailing jet, the luminosity of the lower channel decreases with altitude and remains bright longer than the transition region revealing another trailing phase characterized by light only in the lower channel, the so-called trailing jet (no beads) (Figure 7d for GJ1). Table 1 and Figure 4 show the duration of this phase for all jets. It lasts from 33 ms for GJ5 to 333 ms for GJ1, while the whole trailing jet lasts around 500 ms (from 300 to 683 ms) as generally observed in GJs [*Kuo et al.*, 2009]. During this phase, leader branches are re-illuminated several times after cloud pulses of light, where the lower channel of the jet disappears. Figure 7e shows an example of this process for GJ1. Most GJ events end with cloud luminosity alone, as indicated in Table 1 and Figure 4. This luminosity exhibits intermittent pulses as observed during the phase preceding the visible jet. This last phase of the GJ events is shorter than the first one, except for GJ3 of which the duration is 633 ms.

[22] Color photographs have been obtained for four GJ events. Those for GJ4 and for GJ5 (the most luminous event) are shown in Figure 11. The jets present a blue trunk and a red streamer-like structure which reveals that the beads retrace existing streamer paths in the transition region. The transition zone of GJ5 is much brighter than that of GJ4. The red color visible above 40 km, as for sprites which are generally produced between 40 km and 90 km, is mostly due to the first positive band of N_2 [*Pasko et al.*, 1997]. The blue color of the lower channel is thought to be mainly due to the first N_2^+ negative ($1NN_2^+$) band and to the second N_2 positive ($2PN_2$) band, as in blue jets [*Wescott et al.*, 1998; *Pasko and George*, 2002]. According to the profile in Figure 11b, the blue trunk also contains enhanced red color and in a lower extent enhanced green color, while the transition region is largely dominated by red color. The top section of the jet and the region between the trunk and the transition zone register only very faintly, owing to their short duration and/or low luminosity, and are not visible in the photograph. A major contribution to

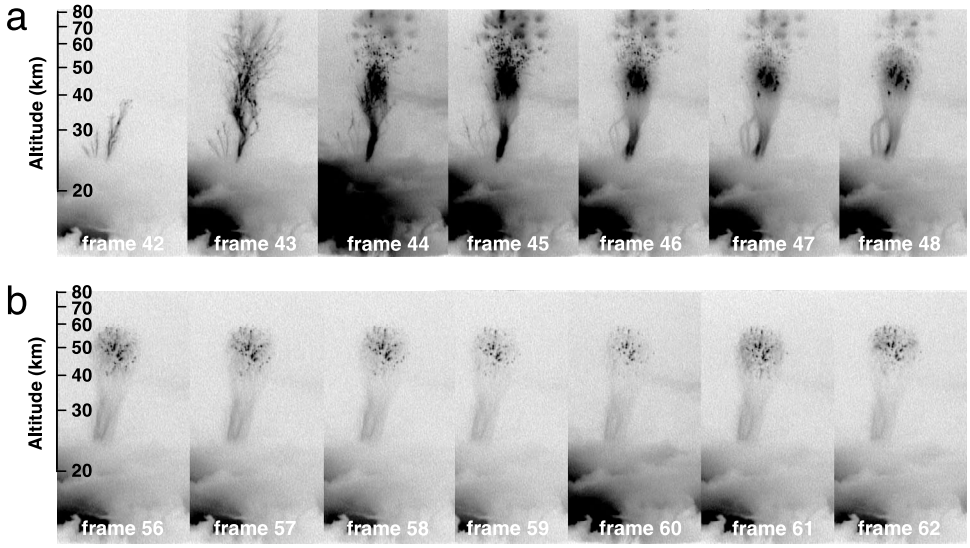

Figure 10. Series of seven successive de-interlaced frames in inverted color from the video imagery of GJ5: (a) t = 684.7–801.6 ms, leading jet/beginning of the trailing jet with beads; and (b) t = 918.5–1035.4 ms, trailing jet with re-brightening (frames 60 and 61). The time reference t = 0 (frame 1) corresponds to the first cloud brightening of the event. The vertical scale is calculated at the distance of the GJs by taking into account the perspective effect and is not valid at the distance of the cloud edge.

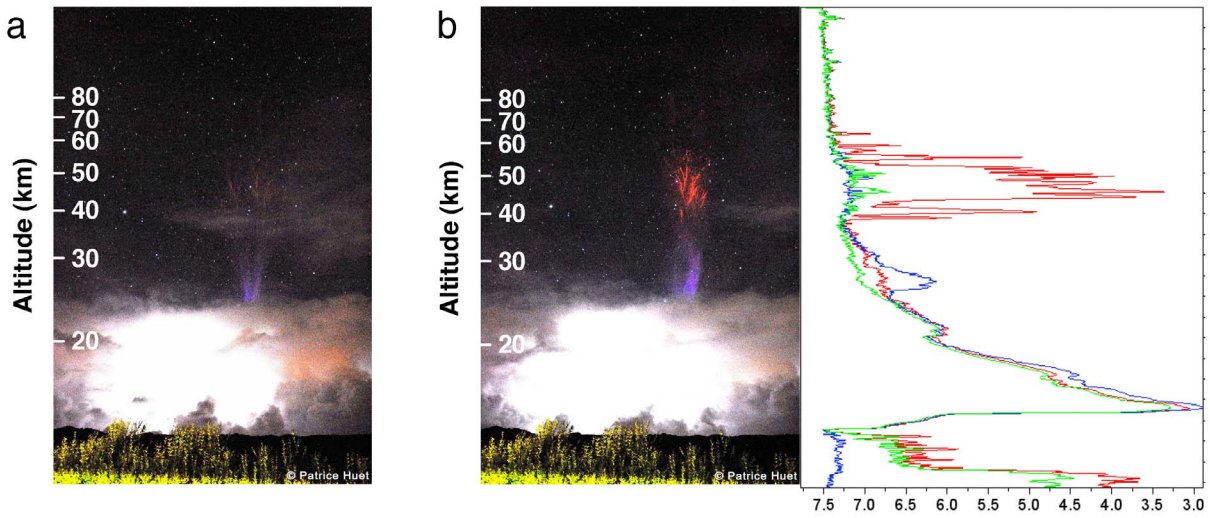

Figure 11. Color photographs (20 s exposure) for (a) GJ4 and (b) GJ5. The right side of Figure 11b shows the vertical profile of the visual magnitude in red, green, and blue channels for GJ5.

the perceived brightness is likely made by the duration of beads in one position, or perhaps by multiple beads retracing streamers. The official visual magnitudes of 63 stars in the photograph have been compared to the green channel values of the Nikon D200 (the green Bayer filter corresponds the most closely to the astronomical V filter). The result is a linear correlation (R^2 = 0.972) which has been used to convert the RGB values of the camera to the magnitude scale. Stars and hot pixels are removed from the image (using a clone stamp tool) and from a narrow slice containing the jet to make the graph in Figure 11b which displays the maximum RGB brightness from every row of the image. For its interpretation, it must be considered that the GJ lasted only for some 400 ms, while light from the stars accumulated over the full 20 s exposure. Therefore, the red transition zone and the blue stem of the jet are in reality a factor of 50 brighter than magnitude 4.5 and 6 to 6.5 in the graph: near magnitude 0 and magnitude 2, respectively. However, if we consider only the green channel, which best approximates human scotopic vision, the jet emits four magnitudes weaker than in the red channel, but would still be perceptible to the dark-adapted human eye. Note that the brightness of individual beads, which move across multiple pixels in the image during this time span, is underestimated and would be easily visible to the eye.

3.3. ELF Signals

[23] ELF transients corresponding to the five GJs have been detected at NCK station. The amplitudes of the GJ related signals are not very high. The signals are the most explicit in the time series of the E_Z field component. In the magnetic records, the signal-to-noise ratio is too low for reliable signal processing. Figure 12 displays the time series of E_Z field components for the five GJs as received at NCK station. Time 0 is shifted to the first peak in each case. The direction of the field jump in the E_Z component at the onset of the event is the same for all events. This direction is consistent with negative charge raised in the cloud in a case of intracloud discharge and from the cloud to the ionosphere in the case of a GJ. According to the timing between the ELF sources and the FDJs (~20 ms except for GJ4 which is 90 ms) and the duration of the cloud discharge before the GJ (>300 ms) from Table 1, the GJs are good candidates to be responsible of the CMC associated with the E_Z jumps. The ELF waveform corresponding to GJ2, GJ3, GJ4, and GJ5 in the E_Z filed component is a double "V," while the waveform corresponding to GJ1 is a triple "V." The double "V" waveform is the most characteristic to source-observer distances near 10,000 km [*Ogawa and Komatsu*, 2009]. The peak-to-peak time delay is practically the same (~100 ms) for GJ2, GJ3, GJ4, and GJ5. It is the time difference between the first and the third peak in the first ELF transient which falls close to the peak-to-peak time delay for the rest

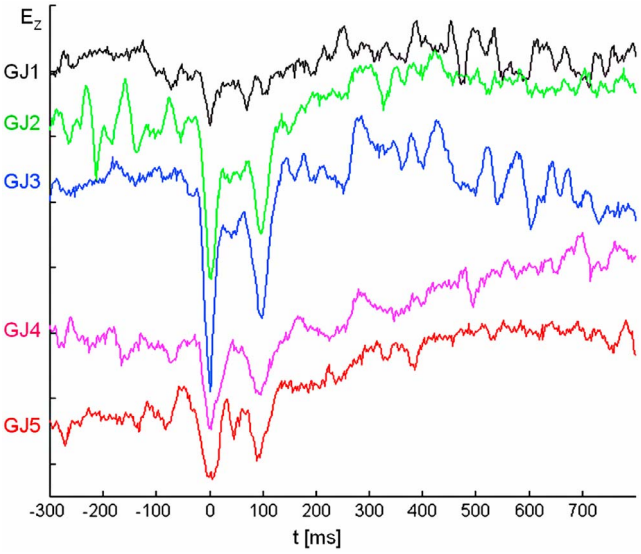

Figure 12. Time series of the E_z field components for the five GJ received at NCK station. Time t = 0 corresponds to the first peak and to the signal production at the source location for each jet.

of the events, so the source of the second peak of the first ELF event is most probably not related to the observed GJs. The two peaks in each event correspond to the direct and the antipodal waves which arrive at the receiving station along the great circle path in opposite direction. This is indicated by the opposite signs of the excursions in the corresponding horizontal magnetic field components.

[24] Since the source-observer distance is known (SOD = 8620 km), the peak-to-peak delay time (P2PDT) allows for the determination of the average group speed of the ELF wave packet in the Earth-ionosphere waveguide and the time of activity of the source of the ELF radiation can be determined, too. Taking the circumference of Earth (CE) as 40,000 km and denoting the group speed of the wave packet in the waveguide as V, the direct wave needs SOD/V time units to reach the observer, while the antipodal wave needs (CE-SOD)/V time units. The difference between these is:

$$\mathrm{P2PDT} = \frac{\mathrm{CE} - \mathrm{SOD}}{\mathrm{V}} - \frac{\mathrm{SOD}}{\mathrm{V}} = \frac{\mathrm{CE} - 2\mathrm{SOD}}{\mathrm{V}} \quad (1)$$

From this, the group velocity can be calculated as:

$$\mathrm{V} = \frac{\mathrm{CE} - 2\mathrm{SOD}}{\mathrm{P2PDT}} \quad (2)$$

Once V is known, the traveling time of the direct wave from the source to the recording station (SOD/V) can be calculated. The calculated group velocities are around 0.8c (c is the speed of light in vacuum) a value characteristic for ELF waves [*Chapman et al.*, 1966]. If this traveling time is extracted from the detection time of the event, the beginning time of the source activity can be determined. It must be noted that the real detection time of the event is generally not the detection time which corresponds to the first peak of the ELF transient. The electronic components of the recording system usually introduce a time delay by causing a phase shift in the incoming signal during its detection. The time delay of the recording system at NCK is 23 ms. The CMCs in the GJs are determined by fitting the analytical spectrum of an exponentially decaying current moment to the measured current moment spectrum [*Huang et al.*, 1999]. The method can be applied successfully to three ELF signals associated with the observed GJs. Owing to the low signal-to-noise ratio in the horizontal magnetic field components, only the time series of vertical electric field component is used to estimate the corresponding CMC. Despite the similar waveforms in the time domain, the procedure has failed to give back valid CMC values for GJ1 and GJ4. In the case of GJ1, the signal is very weak and its spectrum is masked by the spectrum of the noisy background. For GJ4, the signal-to-noise ratio is adequate, still the fit is poor so that the approximation of exponentially decaying current moment probably cannot be applied here. The other three events process well and the resulting CMC is 2800 C km for GJ2, 8100 C km for GJ3, and 1900 C km for GJ5, in absolute values.

4. Discussion

[25] Three of the observed GJs are produced before the end of the vertical development of the storm and two after the beginning of its horizontal expansion. This expansion seems to be due to the development of the storm anvil because very few strokes occur within and most of strokes remain in a very restricted area, the probable convective region. ELF data recorded at NCK show these GJs raised negative charge, as most cases analyzed in the literature [*Su et al.*, 2003; *Krehbiel et al.*, 2008; *Cummer et al.*, 2009]. In a storm with a normal charge structure [*Williams*, 1989], a negative GJ develops above the cloud top after a cloud discharge is triggered between unbalanced lower negative and upper positive charges according to *Krehbiel et al.* [2008] and *Riousset et al.* [2010]. They propose the imbalance is due to the mixing of the upper positive charge and the negative charge from the screening layer at the top of the cloud. They consider before everything the discharge type which occurs in the thundercloud is determined by the location where the breakdown is triggered first. For the first three GJs produced during the vertical development of the thundercloud, one can speculate that during rapid ascent of the buoyant cloud a negative screening charge layer cannot develop and instead will be immediately mixed with the developing upper charge layer. In order to explain the unbalanced charges, the model of tripole of the cloud charge can be considered [*Williams*, 1989]. As a matter of fact, both laboratory experiments and field measurements lead to this tripole model at a macroscopic scale. In this model, the mid level negative charge is larger because it accumulates charge produced by the non inductive charging process at two different levels of temperature. At warmer temperature (below) the ice crystals are negative and they ascend while at colder temperature (above) the graupels are negative and they descend [*Takahashi*, 1978; *Saunders et al.*, 1991]. These conditions favorable for GJ production might last very short time. For the two last GJs produced, the mixing effect can work at the cloud top but also the positive charge can be shifted by horizontal advection. The expansion was stronger in the eastward direction relative to the almost stationary active cells of the storm, which could indicate also a role for vertical wind shear in the upper regions of the storm, as described by *van der Velde et al.* [2010]. Figure 2c displays some scattered CG flashes in the eastern part of the thundercloud which can support this transport of positive charge at upper level. However, a hodograph extracted from the Global Forecasting System model (from the National Centers for Environmental Prediction, USA) shows that the present case occurred in an environment with a bulk shear vector of a moderate 16 m s^{-1} between surface (or cloud base) and cloud top winds, which is only half that of the winter GJ case analyzed by *van der Velde* [2010]. Both effects can be efficient for the reduction of the upper positive cloud charge relative to the main negative charge but it is difficult to estimate their proper contribution.

[26] No other TLE was observed during the lifetime of the present storm likely in most cases of GJs previously reported. As reported by *van der Velde et al.* [2010], different types of TLEs (elves and sprites) were produced by a winter GJ parent storm. In the present case, according to the proximity of the storm, the probability that other types of TLE could have been missed by the camera is very low. In the work of *van der Velde et al.* [2007] other TLEs occurred during the late stages of the storm. In the present storm the video camera monitored the lightning activity until the end of the storm activity (the last CG flash was detected at

19:18:44 UT by the WWLLN). The storm was therefore only specifically favorable for the production of GJs.

[27] The GJs are preceded by a long, intermittent in-cloud luminosity observed in the video imagery, and for most of them without any flash detection by the WWLLN (with the restriction due to the low detection efficiency of WWLLN). Two strokes are detected only at about 0.4 s before GJ3. This luminous activity is therefore consistent with IC discharges of which leaders can propagate out of the cloud and become GJs, by neutralizing charge within the cloud (similar to the concept from *Krehbiel et al.* [2008]). Furthermore, at a larger time scale, all present GJs are preceded by periods of a few tens of seconds without any flash detected by the WWLLN while optical flashes are recorded in the video imagery. *van der Velde et al.* [2010] also noted IC detection associated with a GJ occurring over a winter storm, after a long period without any CG flash detection. Another study by *van der Velde et al.* [2007] exhibited a period without any –CG flashes during several minutes before the GJ, but an increase of +CG flashes (around +15 kA) was detected before the GJ, by the National Lightning Detection Network. These could actually have been IC flashes instead, because of the possible misidentification by the detection system. Our observations also suggest that CG flashes need to cease before a GJ can occur because they tap large amounts of charge from the same source [*Krehbiel et al.*, 2008; *Riousset et al.*, 2010]. So, the present observations clearly show the systematically associated IC discharges before the GJ occurrences and support the theory proposed by *Krehbiel et al.* [2008] and *Riousset et al.* [2010].

[28] The videos for all GJs provide images with details never seen before for these luminous events. The leading jet phase is found to have the most variable duration as indicated in Table 1 and Figure 3. The shortest leading jet is visible in two successive frames which do not allow an accurate estimate of velocity. With such short duration and according to the vertical extent observed, the average velocity could be of the order of 10^6 m s^{-1}, values also estimated by *Su et al.* [2003] from several cases of GJs. Our observations, especially that of the event with the longest leading jet, clearly show the upward velocity is not constant at all during the jet propagation. The upper part of the leading jet propagates at larger velocities. So, the leading jet starts with several visible channels above the cloud, some of them rising and markedly accelerating above about 50 km to reach velocities of the order of 10^6–10^7 m s^{-1}. This range of values was sometimes considered as typical for the leading jet propagation, reported in previous cases probably because at large distance a jet of low brightness can remain invisible [*van der Velde et al.*, 2010]. The velocity of the slowest GJ case (~10^5 m s^{-1}) is of the order of that found by *Pasko et al.* [2002].

[29] When the FDJ is reached, the jet and the cloud exhibit a luminosity increase with variable intensity for all events. This increase of light was previously considered to have a strong analogy with the "return stroke" in CG flashes [*Su et al.*, 2003; *Kuo et al.*, 2009; *Chou et al.*, 2010]. However, not all jets exhibited this return stroke-like process according to *Kuo et al.* [2009]. The present study shows also the occurrence of intense luminosity in the jet at the FDJ is not clearly observed for all jets. At this stage, the top of the jet can include carrot sprite-like patches of light and/or a multitude of beads. This structure at the top of the jet is not always visible and its duration is largely variable when it appears. Its brightness and its duration seem to be related to that of the jet, since it is more visible and more enduring for the most luminous jets (GJ3 and GJ5). Before disappearing, it can coexist with the bright transition region during the trailing jet. The trailing phase is the longest of the jet (from 80% to 91% of the total duration of the visible jet as indicated in Table 1). As illustrated in Figure 6 for GJ5, during this phase the luminosity continuously decreases in the cloud and in two distinct regions of the jet: the blue lower main channel (around 20–40 km altitude) of which the luminosity decreases with altitude, and the transition zone (around 40–65 km) with red luminous beads rising at low velocity (~10^4 m s^{-1}) and retracing original leading jet channels. The beads were initially superposed on a bright glow with unresolved details, and in a later stage, groups of streamers occurred just under the level of the bright beads, very pronounced in GJ4 and GJ5. The polarity and the morphological development of the present GJs show they correspond to the first category proposed by *Chou et al.* [2010].

[30] The upward progress of the beads at a low speed compared with that of a streamer process, suggests the occurrence of streamer-leader processes in the trailing jet as previously proposed by *Kuo et al.* [2009] and as assumed for in the blue jets [*Raizer et al.*, 2006, 2007]. The transition region was considered as a secondary TLE propagating upward while the ionosphere boundary, lowered by the ionization of the FDJ, recovers to a higher altitude [*Kuo et al.*, 2009]. The same mechanism of secondary TLE (in the form of "palm trees") has been described for sprites [*Marshall and Inan*, 2007]. The present observations show that during the overall decrease of the luminosity of the cloud and of these different regions of the trailing jet, a weak re-illumination can occur within the cloud and in the trailing jet regions with a very short delay (<16.7 ms). The trailing phase of the jet exhibits an analogy with the continuing current generally observed after the return stroke of a positive CG flash, with possible superimposed M components as shown by *Thottappillil et al.* [1995] for triggered lightning. The weak re-illumination strongly resembles that produced by M components during the continuing current of CG flashes. This continuing current together with the impulsive leading jet can be an effective source of the detected ELF band radiation. The detection of the waves reaching the observer via the longer great circle path suggests that the intensity of the radiation was strong in the frequency band of the lowest Schumann resonances in these cases. The secondary ELF waves cannot always be observed in earlier low-frequency observations [*Cummer et al.*, 2009] and in some cases no ELF signals associable with the GJ can be detected at all [*Su et al.*, 2003]. This indicates that electric currents in different GJs can exhibit great variation which can considerably affect the spectrum of the emitted electromagnetic radiation and consequently the detectability of these events.

5. Conclusion

[31] Five GJs produced by an isolated tropical storm have been analyzed in terms of conditions of production and luminous characteristics. The storm located east of Réunion

Island developed over sea surface and continuously grew in size during 2 h to about 8000 km^2. The cloud top reached a temperature colder than −81°C. The short distance of observation (around 50 km) allowed recording light from cloud and from the different parts of the jet in unprecedented details and for the first time with color photograph camera. The main observations can be summarized as follows:

[32] 1. The GJs are grouped within two periods of production separated by 40 min and at two different stages of the storm development. These periods are characterized by low CG flash rates compared to other periods of the whole lifetime of the storm and furthermore, the CG lightning activity is observed to cease a few tens of seconds before the jets.

[33] 2. All present GJs are preceded by intermittent optical flashes from the cloud, most of time without any CG flash simultaneously detected, which suggests they originate mainly as intracloud discharges and without any charge transfer to Earth. Furthermore, electric field jumps from ELF data, well synchronized with the jet mechanism, suggest that the sources are the GJs themselves and supports that they carry negative charge to the ionosphere. The CMCs in GJs are probably superior to the CMCs in the body of sprites, which was reported by *Cummer* [2003] to be ~1200 C km or more.

[34] 3. The leading jet has the most variable duration (33 to 167 ms) and becomes much faster above an altitude of 40 km.

[35] 4. During the trailing jet a continuous decrease of luminosity with possible rebrightening is simultaneously observed in different parts of the jet (lower channel, transition zone and for most events carrot sprite-like top) and in the cloud.

[36] 5. The lower channels (20–40 km altitude) produce blue luminosity which decreases with altitude and become more and more diffuse with time. The transition zone (around 40–65 km) consists of bright red luminous beads slowly going up (~10^4 m s^{-1}) by retracing the initial leading jet channels.

[37] **Acknowledgments.** The authors thank Earle Williams for his very helpful comments and remarks on the paper. They thank also two anonymous reviewers for their useful and interesting remarks. The authors wish to thank the World Wide Lightning Location Network (http://wwlln.net/), a collaboration among over 40 universities and institutions, for providing the lightning location data used in this study. The authors thank Jean-Pierre Olry from SATMOS for providing Meteosat observations. The contribution of Serge Soula to this work was supported by the Centre National d'Etudes Spatiales (CNES). The contribution of József Bór was supported by the Hungarian Scientific Research Fund (support ID K72474). The contribution of Oscar van der Velde and Joan Montanyà was possible thanks to grant AYA2009-14027-C05-05 from the Spanish Ministry of Science and Innovation.

References

Chapman, F. W., D. Llanwyn Jones, J. D. W. Todd, and R. A. Challinor (1966), Observation on the propagation constant of the Earth-ionosphere waveguide in the frequency band 8 kc/s to 16 kc/s, *Radio Sci.*, *1*, 1273.

Chen, A. B., et al. (2008), Global distributions and occurrence rates of transient luminous events, *J. Geophys. Res.*, *113*, A08306, doi:10.1029/2008JA013101.

Chou, J. K., et al.. (2010), Gigantic jets with negative and positive polarity streamers, *J. Geophys. Res.*, *115*, A00E45, doi:10.1029/2009JA014831.

Cummer, S. A. (2003), Current moment in sprite-producing lightning, *J. Atmos. Sol. Terr. Phys.*, *65*, 499, doi:10.1016/S1364-6826(02)00318-8.

Cummer, S. A., and U. S. Inan (2000), Modeling ELF radio atmospheric propagation and extracting lightning currents from ELF observations, *Radio Sci.*, *35*, 385, doi:10.1029/1999RS002184.

Cummer, S. A., J. Li, F. Han, G. Lu, N. Jaugey, W. A. Lyons, and T. E. Nelson (2009), Quantification of the troposphere-to-ionosphere charge transfer in a gigantic jet, *Nat. Geosci.*, *2*, 617, doi:10.1038/ngeo607.

Hobara, Y., M. Hayakawa, E. Williams, R. Boldi, and E. Downes (2006), Location and electrical properties of sprite-producing lightning from a single ELF site, in *Sprites, Elves and Intense Lightning Discharges*, *NATO Sci. Ser. II: Math. Phys. and Chem.*, vol. 225, edited by M. Fullekrug, E. A. Mareev, and M. J. Rycroft, p. 211, Springer, New York.

Huang, E., E. Williams, R. Boldi, S. Heckman, W. Lyons, M. Taylor, T. Nelson, and C. Wong (1999), Criteria for sprites and elves based on Schumann resonance observations, *J. Geophys. Res.*, *104*, 16,943, doi:10.1029/1999JD900139.

Krehbiel, P. R., J. A. Riousset, V. P. Pasko, R. J. Thomas, W. Rison, M. A. Stanley, and H. E. Edens (2008), Upward electrical discharges from thunderstorms, *Nat. Geosci.*, *1*, 233, doi:10.1038/ngeo162.

Kuo, C.-L., et al. (2009), Discharge processes, electric field, and electron energy in ISUAL-recorded gigantic jets, *J. Geophys. Res.*, *114*, A04314, doi:10.1029/2008JA013791.

Lay, E. H., A. R. Jacobson, R. H. Holzworth, C. J. Rodger, and R. L. Dowden (2007), Local time variation in land/ocean lightning flash density as measured by the World Wide Lightning Location Network, *J. Geophys. Res.*, *112*, D13111, doi:10.1029/2006JD007944.

Marshall, R. A., and U. S. Inan (2007), Possible direct cloud-to-ionosphere current evidenced by sprite-initiated secondary TLEs, *Geophys. Res. Lett.*, *34*, L05806, doi:10.1029/2006GL028511.

Mazur, V., and L. Ruhnke (1998), Model of electric charges in thunderstorms and associated lightning, *J. Geophys. Res.*, *103*, 23,299, doi:10.1029/98JD02120.

Nickolaenko, A. P., M. Hayakawa, and Y. Hobara (2010), Q-bursts: Natural ELF radio transients, *Surv. Geophys.*, *31*, 409, doi:10.1007/s10712-010-9096-9.

Ogawa, T., and M. Komatsu (2009), Q-bursts from various distances on the Earth, *Atmos. Res.*, *91*, 538, doi:10.1016/j.atmosres.2008.04.013.

Pasko, V. P., and J. J. George (2002), Three-dimensional modeling of blue jets and blue starters, *J. Geophys. Res.*, *107*(A12), 1458, doi:10.1029/2002JA009473.

Pasko, V. P., U. S. Inan, T. F. Bell, and Y. N. Taranenko (1997), Sprites produced by quasi-electrostatic heating and ionization in the lower ionosphere, *J. Geophys. Res.*, *102*, 4529, doi:10.1029/96JA03528.

Pasko, V. P., M. A. Stanley, J. D. Mathews, U. S. Inan, and T. G. Wood (2002), Electrical discharge from a thundercloud top to the lower ionosphere, *Nature*, *416*, 152, doi:10.1038/416152a.

Raizer, Y. P., G. M. Milikh, and M. N. Shneider (2006), On the mechanism of blue jet formation and propagation, *Geophys. Res. Lett.*, *33*, L23801, doi:10.1029/2006GL027697.

Raizer, Y. P., G. M. Milikh, and M. N. Shneider (2007), Leader streamers nature of blue jets, *J. Atmos. Sol. Terr. Phys.*, *69*, 925, doi:10.1016/j.jastp.2007.02.007.

Rakov, V. A., and M. A. Uman (2003), Lightning Physics and Effects, *Cambridge Univ. Press*, Cambridge, U. K.

Riousset, J. A., V. P. Pasko, P. R. Krehbiel, W. Rison, and M. A. Stanley (2010), Modeling of thundercloud screening charges: Implications for blue and gigantic jets, *J. Geophys. Res.*, *115*, A00E10, doi:10.1029/2009JA014286.

Rodger, C. J., S. Werner, J. B. Brundell, E. H. Lay, N. R. Thomson, R. H. Holzworth, and R. L. Dowden (2006), Detection efficiency of the VLF World Wide Lightning Location Network (WWLLN): Initial case study, *Ann. Geophys.*, *24*, 3197, doi:10.5194/angeo-24-3197-2006.

Sátori, G. (2007), Schumann resonance observations, in *Geophysical Observatory Reports of the Geodetic and Geophysical Research Institute of the Hungarian Academy of Sciences*, edited by V. Wesztergom, pp. 75–80, Nagycenk Geophys. Obs., Nagycenk, Hungary.

Sátori, G., J. Szendrői, and J. Verő (1996), Monitoring Schumann resonances. 1. Methodology, *J. Atmos. Terr. Phys.*, *58*, 1475, doi:10.1016/0021-9169(95)00145-X.

Saunders, C. P.R., W. D. Keith, and R. P. Mitzeva (1991), The effect of liquid water on thunderstorm charging, *J. Geophys. Res.*, *96*, 11,007.

Sivakumar, V., J.-L. Baray, S. Baldy, and H. Bencherif (2006), Tropopause characteristics over a southern subtropical site, Reunion Island (21°S, 55°E): Using radiosonde-ozonesonde data, *J. Geophys. Res.*, *111*, D19111, doi:10.1029/2005JD006430.

Su, H.-T., et al. (2003), Gigantic jets between a thundercloud and the ionosphere, *Nature*, *423*, 974, doi:10.1038/nature01759.

Takahashi, T. (1978), Riming electrification as a charge generation mechanism in thunderstorms, *J. Atmos. Sci.*, *35*, 1536, doi:10.1175/1520-0469(1978)035<1536:REAACG>2.0.CO;2.

Thottappillil, R., J. Goldberg, V. Rakov, M. Uman, R. Fisher, and G. Schnetzer (1995), Properties of M components from currents measured at triggered lightning channel base, *J. Geophys. Res.*, *100*, 25,711, doi:10.1029/95JD02734.

van der Velde, O. A., W. A. Lyons, T. E. Nelson, S. A. Cummer, J. Li, and J. Bunnell (2007), Analysis of the first gigantic jet recorded over continental North America, *J. Geophys. Res.*, *112*, D20104, doi:10.1029/2007JD008575.

van der Velde, O. A., J. Bór, J. Li, S. A. Cummer, E. Arnone, F. Zanotti, M. Füllekrug, C. Haldoupis, S. NaitAmor, and T. Farges (2010), Multi-instrumental observations of a positive gigantic jet produced by a winter thunderstorm in Europe, *J. Geophys. Res.*, *115*, D24301, doi:10.1029/2010JD014442.

Wescott, E. M., D. Sentman, D. Osborne, D. Hampton, and M. Heavner (1995), Preliminary results from the Sprites94 aircraft campaign: 2. Blue jets, *Geophys. Res. Lett.*, *22*, 1209, doi:10.1029/95GL00582.

Wescott, E. M., D. D. Sentman, M. J. Heavner, D. L. Hampton, and O. H. Vaughan Jr. (1998), Blue Jets: Their relationship to lightning and very large hailfall, and physical mechanisms for their production, *J. Atmos. Sol. Terr. Phys.*, *60*, 713, doi:10.1016/S1364-6826(98)00018-2.

Wescott, E. M., D. D. Sentman, H. C. Stenbaek-Nielsen, P. Huet, M. J. Heavner, and D. R. Moudry (2001), New evidence for the brightness and ionization of blue starters and blue jets, *J. Geophys. Res.*, *106*, 21,549, doi:10.1029/2000JA000429.

Williams, E. R. (1989), The tripole structure of thunderstorms, *J. Geophys. Res.*, *94*, 13,151.

Williams, E. R., et al. (2010), Ground-based detection of sprites and their parent lightning flashes over Africa during the 2006 AMMA campaign, *Q. J. R. Meteorol. Soc.*, *136*, 257.

C. Barthe, Laboratoire de l'Atmosphère et des Cyclones, Université de la Réunion, CNRS, Météo-France, 15 avenue René Cassin – BP 7151, Université de la Réunion, F-97715 Saint-Denis, France.

J. Bór, Geodetic and Geophysical Research Institute, Hungarian Academy of Sciences, Csatkai u. 6-8, H-9400 Sopron, Hungary.

P. Huet, La Maison du Volcan, Muséum de la Fournaise, RN3 Bourg-Murat, F-97418 Plaine-des-Cafres, France.

J. Montanya and O. van der Velde, Electrical Engineering Department, Technological University of Catalonia, Colon, 1 Terrassa, E-08222 Barcelona, Spain.

S. Soula, Laboratoire d'Aérologie, Université de Toulouse, CNRS, 14 avenue Edouard Belin, F-31400 Toulouse, France. (sous@aero.obs-mip.fr)